Carbon Nanodot Solar Cells from Renewable Precursors

Adam Marinovic[1], Lim Swee Kiat[2], Steve Dunn[1], Maria-Magdalena Titirici[1*] and Joe Briscoe[1*],

1. Materials Research Institute, Queen Mary University of London, Mile End Road, E14NS, London
2. National University of Singapore, Faculty of Engineering, 9 Engineering Drive 1, Singapore 117575

*Corresponding authors: m.m.titirici@qmul.ac.uk ; j.briscoe@qmul.ac.uk

Abstract

It has recently been shown that waste biomass can be converted into a wide range of functional materials, including those with desirable optical and electronic properties, offering the opportunity to find new uses for these renewable resources. Photovoltaics is one area where finding the combination of abundant, low-cost and non-toxic materials with the necessary functionality can be challenging. In this paper we compare the performance of carbon nanodots derived from a wide range of biomaterials obtained from different biomass sources as sensitizers for TiO_2-based nanostructured solar cells; polysaccharides (chitosan and chitin), monosaccharide (D-glucose), amino acids (L-arginine and L-cysteine) and raw lobster shells are all used to produce carbon nanodots via hydrothermal carbonisation. The highest solar power conversion efficiency (PCE) of 0.36 % was obtained by using L-arginine carbon nanodots as sensitizers, while lobster shells, as a model source of chitin from actual food waste, showed a PCE of 0.22 %. By comparing this wide range of materials, we have correlated the performance of the solar cells with the materials characteristics by carefully investigating the structural and optical properties of each family of carbon nanodots, and have shown that the combination of amine and carboxylic acid functionalisation is particularly beneficial for the solar cell performance.

Keywords: photovoltaic, carbon quantum dot, biomass, hydrothermal carbonisation, food waste

Introduction

A big challenge in materials research for sustainable energy generation is to develop new, advanced materials with good optical and electrical properties that will enable us to develop highly efficient, mass-producible and inexpensive photovoltaics (PVs). In order to achieve this, it should avoid the use of expensive and rare elements,[1] in addition to avoiding toxic materials that could be harmful if released into the environment.

Third generation PVs aim to reduce the production costs, and/or obtain power conversion efficiencies greater than the Shockley-Queisser limit[2] by utilizing advanced photovoltaic concepts such as multi-junction solar cells, hot electron injection and multi-exciton generation.[3] Technologies that aim for lower production cost include dye-sensitized solar cells (DSSC)[4], organic photovoltaics[5,6], perovskite solar cells[7] and quantum dot solar cells[8].

DSSCs are usually composed of a mesoporous wide band-gap semiconductor (TiO_2, ZnO), which is sensitized with a light-absorbing dye (often based on an organic ruthenium complex), a redox electrolyte (I_3^-/I^- redox couple, polysulfide redox couple or solid-state electrolyte) and a counter electrode (Pt, or earth-abundant alternatives).[1,9] This structure has been developed into new directions by replacing the light absorbing dye with alternative materials, such as semiconductor quantum dots to develop quantum dot sensitized solar cells (QDSSC).[3,10] These aim to access the tunable band gap and band levels of QDs to enhance light absorption and charge extraction in the structure, particularly in the infra-red.[11,12] Until recently they achieved around 9% efficiency,[13–19] but have now surpassed 11% [20]. However, QDSSCs are mainly fabricated using highly toxic cadmium (Cd) and lead (Pb) chalcogenide elements[10,21,22] This makes their implementation problematic because of health and environmental issues, a problem also currently shared by perovskite solar cells. There has recently been progress in producing high-efficiency QDSSCs using non-toxic materials, such as using $(CuInSe_2)_{1-x}(ZnSe)_x$ QDs, giving 11.6% efficiency [23]. However, these still use indium, a scarce and expensive element that already is in high-demand, particularly for display applications.

An alternative class of material that has recently been investigated as a sensitizer in mesostructured solar cells is carbon nanodots (CNDs), sometimes referred to as carbon quantum dots (CQDs), or simply carbon dots.[24,25] CNDs are generally defined as quasi-spherical carbon nanoparticles with sizes around 10 nm in diameter consisting of sp^2/sp^3 carbon cores and different functional groups on the surface. They possess low toxicity, cheap and easy synthesis, and can show excitation-dependent or independent fluorescence emission and size-dependent fluorescence emission.[26,27] They can also be derived from a wide range of naturally-occurring organic materials (biomass), including biomass that is otherwise regarded as waste.[28–30] In conventional semiconductor quantum dots band gap absorption and photoluminescence are determined by the quantum confinement effect, whereas in CNDs the origins of photoluminescence are determined by the core states and by the molecular states of functional groups on the surface of CNDs.[31–33] Therefore, CNDs offer an interesting possibility of

tuning their optical and electrical properties by varying their structure and functional groups, while using non-toxic, abundant and potentially waste-derived materials.

The concept of using graphitic carbon nanoparticles as sensitizers for mesostructured solar cells was first demonstrated by Yan *et al.* in 2010, who used graphene quantum dots (GQDs) as sensitizers in a mesoporous TiO_2 solar cell[34]. The GQDs were obtained by the cleaving and capping of graphene sheets, which were then adsorbed onto the TiO_2, giving a solar cell efficiency of 0.056%. Following this were the first reports of CND-sensitised solar cells (CNDSSCs) produced using solution synthesis of carbon-containing chemical precursors. Mirtchev *et al.* used γ-butyrolactone to produce CNDs for sensitisation of mesoporous TiO_2 solar cells in 2012 [35], and Zhang *et al.* used a combination of CCl_4 and $NaNH_2$ to produce CNDs for solar cells [36]. In both cases efficiencies of 0.13% were produced, and in the latter case it was shown that N-doping of the CNDs gave significantly improved performance compared to non-doped CNDs. More recently, CNDs derived from biomass or waste organic materials have been investigated for this application; we previously used CNDs derived from the hydrothermal carbonisation of biomass-derived precursors (glucose, chitin and chitosan) as sensitizers in solar cells, producing a solid-state cell based on ZnO nanorods and CuSCN.[37] However, we found that the light absorption was a clear limiting factor when using the relatively low surface area ZnO nanorods, and could not be increased by building up thicker layers of the CNDs, similarly to conventional DSSCs. This indicated that the more conventional mesoporous TiO_2, liquid-state DSSC architecture would be more suitable for CNDSSCs, as reported in other work. Following this have been a number of reports of CNDSSCs using biomass-derived materials, including CNDs derived from the hydrothermal carbonisation of monkey grass, which gave an efficiency of 0.53% [38]. Interestingly it was found that the efficiency could be increased to this level from 0.18% by using an aqueous iodide electrolyte in the cell rather than acetonitrile-based electrolyte, which was linked to a quenching of the fluorescence of the CNDs leading to improved charge transfer into the TiO_2. Margraf *et al.* recently reported CNDSSCs with an efficiency of 0.24% using CNDs derived from citric acid, urea and formic acid[39]. It was shown through time-resolved measurements that despite producing CNDs with absorption extending into the visible, these states did not contribute to the photocurrent as they acted as trap states, highlighting the challenge of extending the CND sensitisation into the visible region, where most of the absorption normally occurs in the UV. Wang *et al.* have also recently used CNDs derived from citric acid in solar cells, adding ammonia to the reaction. They achieved the highest-reported efficiency of 0.79% [40]. They suggest that the N-doping of the CNDs may again be beneficial, but unfortunately provide no control comparison without N, and report data from only one solar cell, therefore it is difficult to draw strong conclusions from this report, including the repeatability of this high efficiency for CND PVs.

Here we investigate the sensitisation of mesoporous TiO_2-based solar cells with CNDs derived from a wide range of renewable, biomass-derived precursors. As well as using mono/polysaccharide

precursors, including those with nitrogen functionality, as in our previous work (glucose, chitosan, chitin), we also investigate the amino acids L-arginine and L-cysteine, where the latter also includes sulphur functionality in the form of a thiol group (see **SI**, **Figure S1**). Furthermore, we show that CNDs can be produced from actual food waste in the form of lobster shells, which were purified, followed by equivalent hydrothermal carbonisation to the other precursors. By investigating a much wider range of precursors than used in other work, we aim to shed light on the link between the varied CND functionalisation that results from the precursor functional groups and the performance of the resulting solar cells. In addition, by using mesoporous TiO_2 we improve on our previous work[37] where, as discussed, surface area was a limiting factor. We show that these biomass-derived precursor materials produce carbon nanodots with sizes in the range of 5-16 nm, with well-defined fluorescence behaviour and surface functionalisation that reflects the functional groups present in the starting material. When used in the mesostructured solar cells we show that there is a clear correlation between this functionalisation and the solar cell efficiency. Those carbon nanodots with high levels of amines combined with carboxylic acid functionalisation, i.e. those derived from amino acids, produce the highest efficiencies, with L-arginine-derived CNDs producing devices with the highest efficiency of 0.36%. This is among the top three highest efficiencies of CNDSSCs demonstrated previously. Strikingly, the solar cells sensitized using CNDs derived from lobster shells obtained as food waste show only slightly lower efficiency of 0.22%, demonstrating the real possibility of using waste products to produce effective optoelectronic materials for use in sustainable energy technologies. Therefore, by surveying a range of biomass-derived CNDs, and demonstrating a clear link between functionalisation and solar cell performance, we provide a guide to direct future development of sustainable, low-cost biomass-derived sensitizers for nanostructured solar cells.

Results and Discussion

Carbon nanodots (CNDs) were produced by the hydrothermal carbonisation of a range of biomass-derived precursors. In brief, 0.7 g of chitosan, chitin, D-(+)-glucose, L-arginine, L-cysteine or purified lobster powder (derived from lobster shells left as food waste – see **Experimental Methods**) in 20 ml of ethanol were heated in an autoclave at 200 °C for 6 hours followed by separation of the liquid phase containing the CNDs. In all cases CNDs were produced with a quasi-spherical morphology, as can be seen from transmission electron microscope (TEM) images (**Figure 1** and **Figure S2**). In the case of glucose, CNDs aggregate into self-assembled structures, as seen in Figure 1b. As we have shown previously,[37] there is a clear influence of the molecular precursor used on the CND size ranging from (5.15 ± 0.83) nm in the case of glucose CNDs to (15.0 ± 2.5) nm for L-arginine CNDs. Average particle diameters for all as-synthesized CNDs are given in **Table S1**.

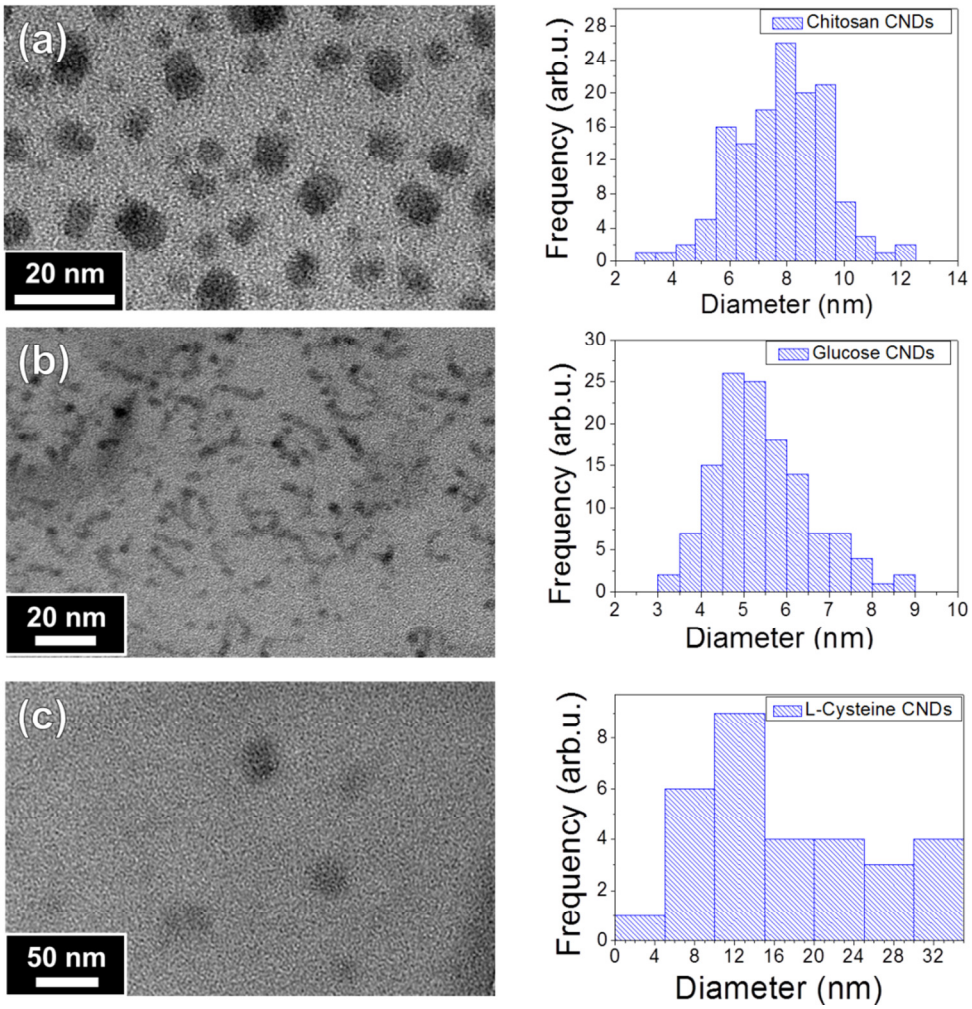

Figure 1 TEM images at 200 kV of as-synthesized carbon nanodots and corresponding size histograms: a) chitosan, b) glucose and c) L-cysteine.

For all CNDs except lobster CNDs, the main structure was found by X-ray diffraction (XRD) analysis to comprise a set of sp^2 graphitic carbons with stacking faults (known as turbostratic carbons) based on a broad 002 peak at about $2\theta = 21°$, while no peak for hexagonal graphite was detected at $2\theta = 12°$ (**Figure 2**). No other peaks were detected in XRD spectrum confirming the amorphous nature of all carbon nanodots. The lobster-derived CNDs show all the features characteristic of the pure lobster powder, which is consistent with the observation that only small fraction of pure lobster powder is soluble during the HTC reaction (**Figure S3**).

The graphitic structure was also confirmed by Raman analysis for chitosan, chitin and glucose CNDs, which demonstrated D and G bands usually found in graphene and graphite,[41,42] with the D-to-G-band intensity ratio and G-band downshift indicating a higher level of disorder than pure graphite (see **SI, Figure S4 and Table S2**). For L-arginine CNDs, L-cysteine CNDs and lobster CNDs, no obvious D

and G bands were detected in the Raman spectra, which may be due to the high fluorescence of these carbon nanodots disturbing the Raman characterization.[43]

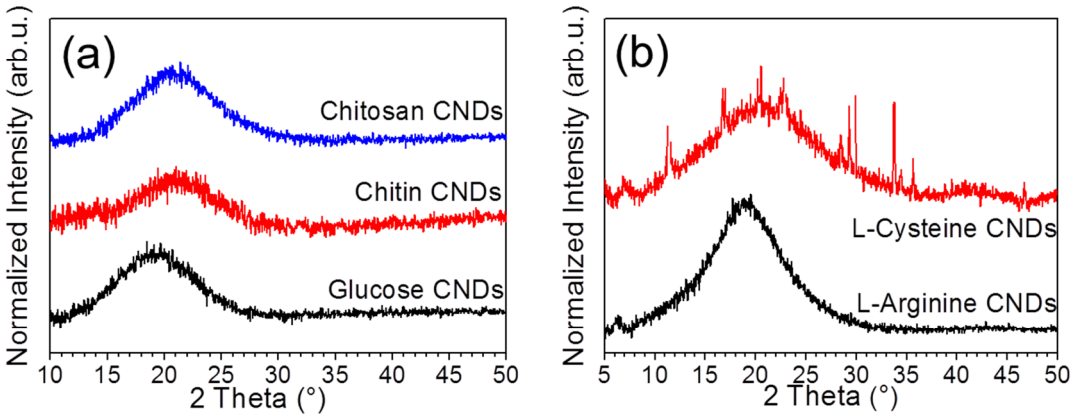

Figure 2 XRD spectra for carbon nanodots: a) chitosan CNDs, chitin CNDs and D-glucose CNDs; b) L-arginine CNDs and L-cysteine CNDs.

Further to the core structural information about the CNDs, as discussed above it is important to ascertain the key functional groups that are present in the CNDs, as they can have a strong impact on the properties. As such, the CNDs were analysed by Fourier Transform Infrared Spectroscopy (FTIR – **Figure S5** and **Table S3**), X-ray photoelectron spectroscopy (XPS – **Figure 3**), and elemental analysis (**Table S5**). Full analysis of these data is included in the **Supporting Information**. This analysis confirmed that the CNDs largely retained the functional groups that were present in the starting material, as found in previous studies.[37] Specifically, FTIR showed stretching mode corresponding to C-O, O-H and N-H for all CNDs (except for glucose in the case of N-H), with C=O also present in glucose and amino acid-derived CNDs. XPS N 1s spectra for all CNDs (except glucose) showed a peak around 399.5-400 eV, associated with amines or amides, which is confirmed as amide in the case of chitin and lobster (which largely contains chitin) due to the presence of amide stretching bands in FTIR, and amine for chitosan and the amino acids. In addition, L-cysteine CNDs show evidence for a thiol group in both XPS analysis of S 2p and FTIR, and 0.63 wt.% S was also measured with elemental analysis (**Table S5**). However, this is much lower than the 26 wt.% S present in L-cysteine, which implies that only a small proportion of the thiol functional groups were retained in the final CNDs. In addition to this evidence for the retention of the surface functional groups from the precursors, XPS also supports the XRD and Raman results that show conversion to a graphitic structure; all C 1s spectra (see **SI, Figure S6**) show peaks around 284.6-285 eV, which correspond to the sp^2/sp^3 carbon of the graphitic structure. In addition, XPS also shows a peak around 398.4 eV in the N 1s spectra for all CNDs (except glucose), which is associated with pyridinic nitrogen, which is likely formed during the synthesis of the CNDs as part of the ring formation.[44]

Thus, to summarise the structural data, all CNDs show evidence of sp^2/sp^3 graphitic carbon, supporting conversion of the precursors to CNDs with a graphitic structure, with pyridinic structures for N-containing CNDs. All CNDs retain -OH groups, likely alcohols for chitin, chitosan and lobster, and carboxylic acid for amino acids and glucose due to the additional presence of C=O (which must form during synthesis for glucose). N-H groups are retained from all N-containing precursors in the form of amide groups for chitin and lobster, and amines for chitosan and amino acids. Finally, L-cysteine has the addition of the thiol group retained from the precursor (though in much smaller proportion). This preservation of some portion of the starting structure is supported by elemental analysis, with N detected in all CNDs except glucose, with the highest proportion in L-arginine-derived CNDs, which have the highest proportion of N in the starting material (**Table S5**).

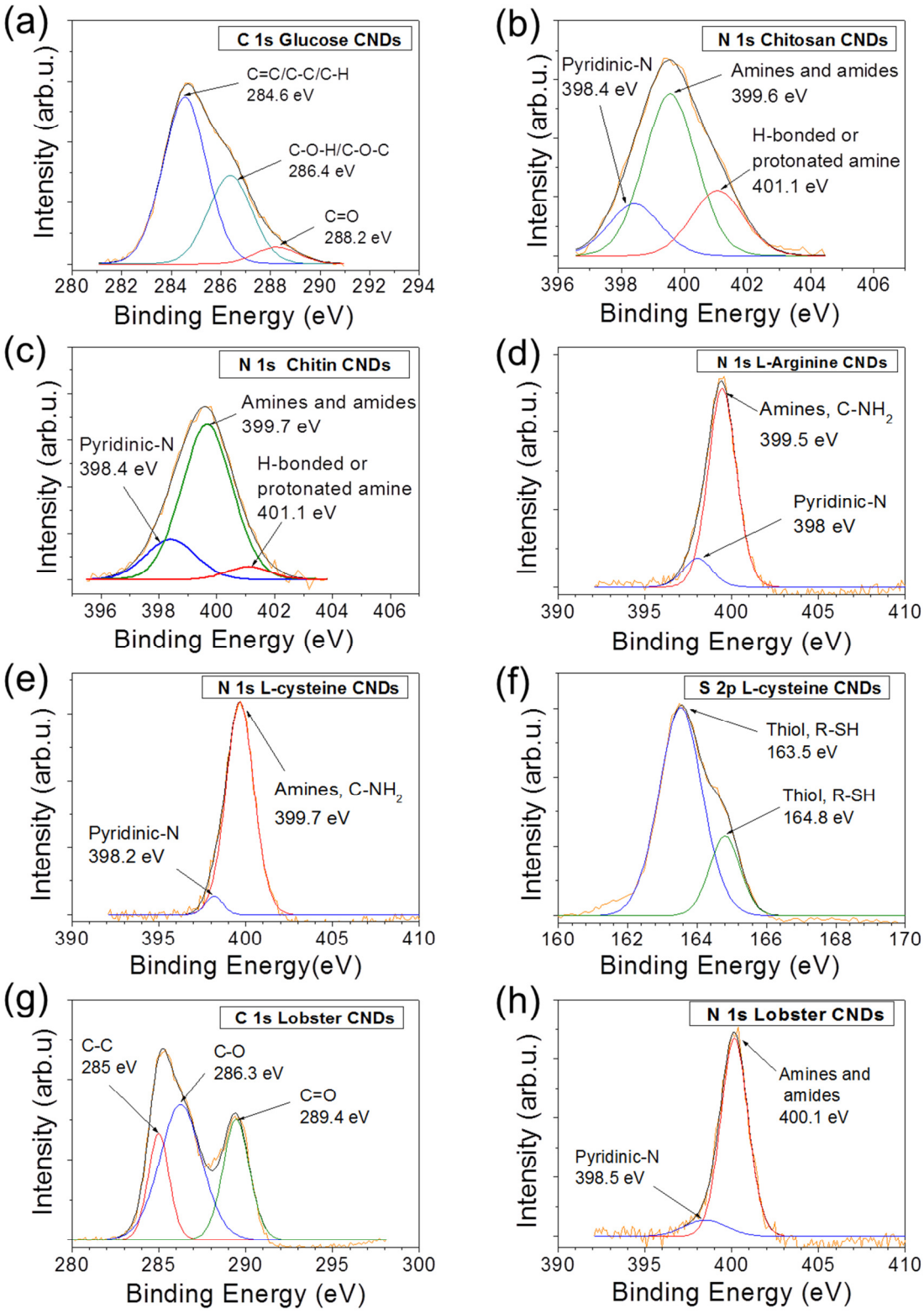

Figure 3 Deconvoluted XPS C 1s peaks of glucose CNDs (a) and lobster CNDs (g); N 1s peaks of chitosan CNDs (b), chitin CNDs (c), L-arginine CNDs (d), L-cysteine CNDs (e) and lobster CNDs (h) and S 2p peaks of L-cysteine CNDs (f).

CNDs produced from all starting materials show excitation-dependent fluorescence, which reflects the complexity of the optical properties of these materials. The normalized absorption, photoluminescence excitation (PLE) and strongest photoluminescence (PL) spectra for all carbon nanodots are shown in **Figure 4**, with the full range of data included in the **Supporting Information (Figure S8)**. Although, with the main portion of the absorption in the UV, these materials are not necessarily ideal as solar cell absorbers, the large absorption tail into the visible and fluorescence that spans a part of the visible range from 400-500 nm (see **SI, Figure S7** and **Figure S8**) indicate that visible transitions do exist, and warrant further investigation. There are also small PL emission peaks at ~800 nm. However, these are most likely caused by Raman scattering of the excitation light, as their position is dependent on the excitation wavelength. The peaks at the excitation wavelength (associated with Rayleigh scattering) have been removed for clarity.

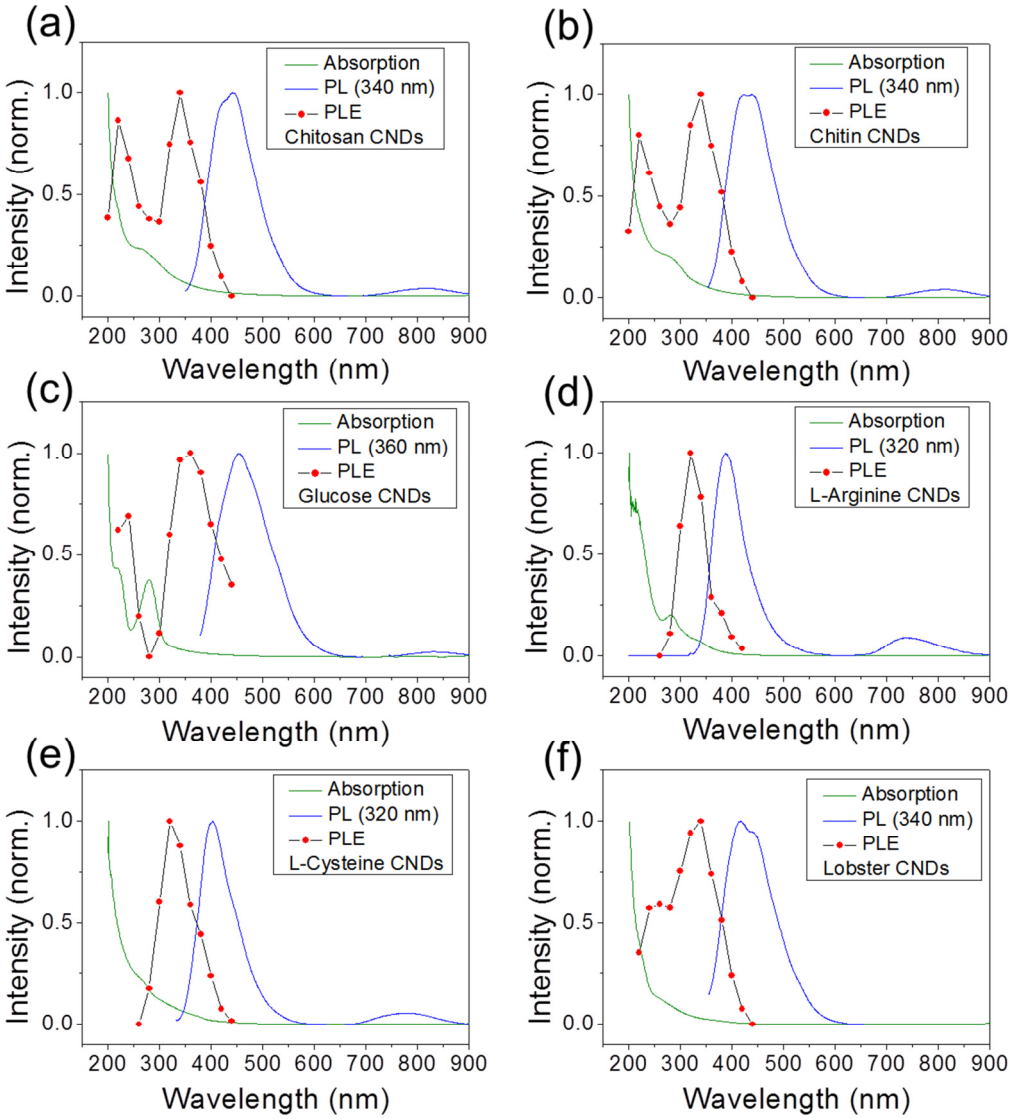

Figure 4 Normalized absorption, photoluminescence excitation (PLE) and strongest photoluminescence (PL) plots for all carbon nanodots (PL excitation wavelength is given in brackets):

(a) chitosan CNDs, (b) chitin CNDs, (c) D-glucose CNDs, (d) L-arginine CNDs, (e) L-cysteine CNDs and (f) lobster CNDs. Intensity shown for PLE spectra is the maximum intensity across the whole emission spectrum at that excitation wavelength. The wavelengths of this emission can be seen in Figure S8.

Solar cells were produced based on a standard DSSC structure by coating each type of CNDs onto a mesoporous TiO_2 (P25) scaffold, and combining with an I_3^-/I^- redox couple and Pt counter electrode (see **Experimental Methods**). The solar-cell current-voltage (*J-V*) curves are shown in **Figure 5** and the corresponding operational parameters are shown in **Table 1** and as box plots in **Figure 6**. To verify the performance parameters of solar cells we produced three devices for each of the carbon nanodots as sensitizers.

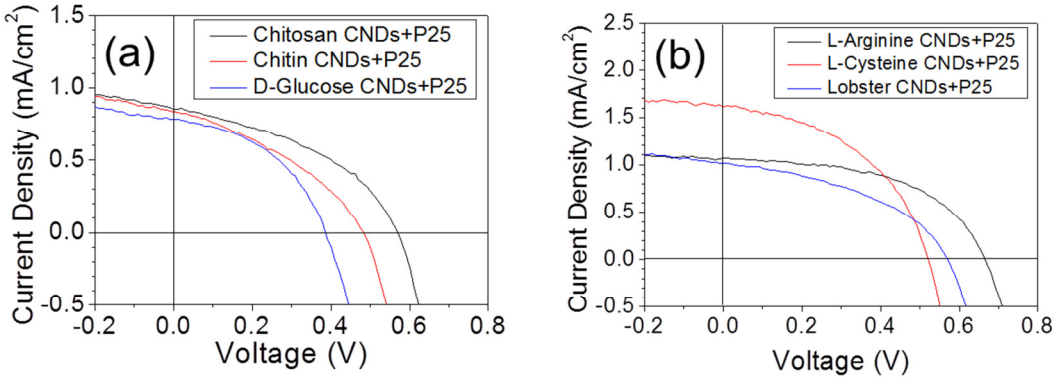

Figure 5 Illuminated current-voltage data for FTO / P25 TiO_2 / CNDs / (I_3^-/I^-) / Pt solar cells: (a) chitosan CNDs, chitin CNDs and D-glucose CNDs; (b) L-arginine CNDs, L-cysteine CNDs and lobster CNDs. Data is shown for the best cells of each type.

Table 1 Solar cell operational parameters for carbon nanodot sensitized TiO_2 (P25) nanostructured solar cells. Averages and errors are taken from three devices per type and three measurements per device.

Sample	**J_{SC} [mA/cm^2]**	**V_{OC} [V]**	**FF**	**PCE [%]**	**R_S [kΩ]**	**R_{SH} [kΩ]**
Non-sensitized TiO_2 (P25)	0.024 ± 0.003	0.493 ± 0.009	0.326 ± 0.004	0.004 ± 0.001	34.7 ± 0.4	113.4 ± 0.9
Chitosan CNDs+P25	0.80 ± 0.03	0.550 ± 0.003	0.38 ± 0.01	0.167 ± 0.008	0.80 ± 0.01	7.5 ± 0.2
Chitin CNDs+P25	0.83 ± 0.01	0.469 ± 0.002	0.357 ± 0.004	0.139 ± 0.002	0.88 ± 0.03	6.8 ± 0.2

D-Glucose CNDs+P25	0.68 ± 0.05	0.410 ± 0.008	0.38 ± 0.02	0.103 ± 0.008	0.94 ± 0.05	4.4 ± 0.2
L-Arginine CNDs+P25	0.97 ± 0.05	0.660 ± 0.003	0.57 ± 0.02	0.362 ± 0.007	0.43 ± 0.02	24.3 ± 1.9
L-Cysteine CNDs+P25	1.43 ± 0.06	0.509 ± 0.005	0.461 ± 0.006	0.34 ± 0.01	0.30 ± 0.02	8.2 ± 0.6
Lobster CNDs+P25	1.05 ± 0.01	0.554 ± 0.003	0.37 ± 0.01	0.216 ± 0.008	0.48 ± 0.03	7.8 ± 0.2

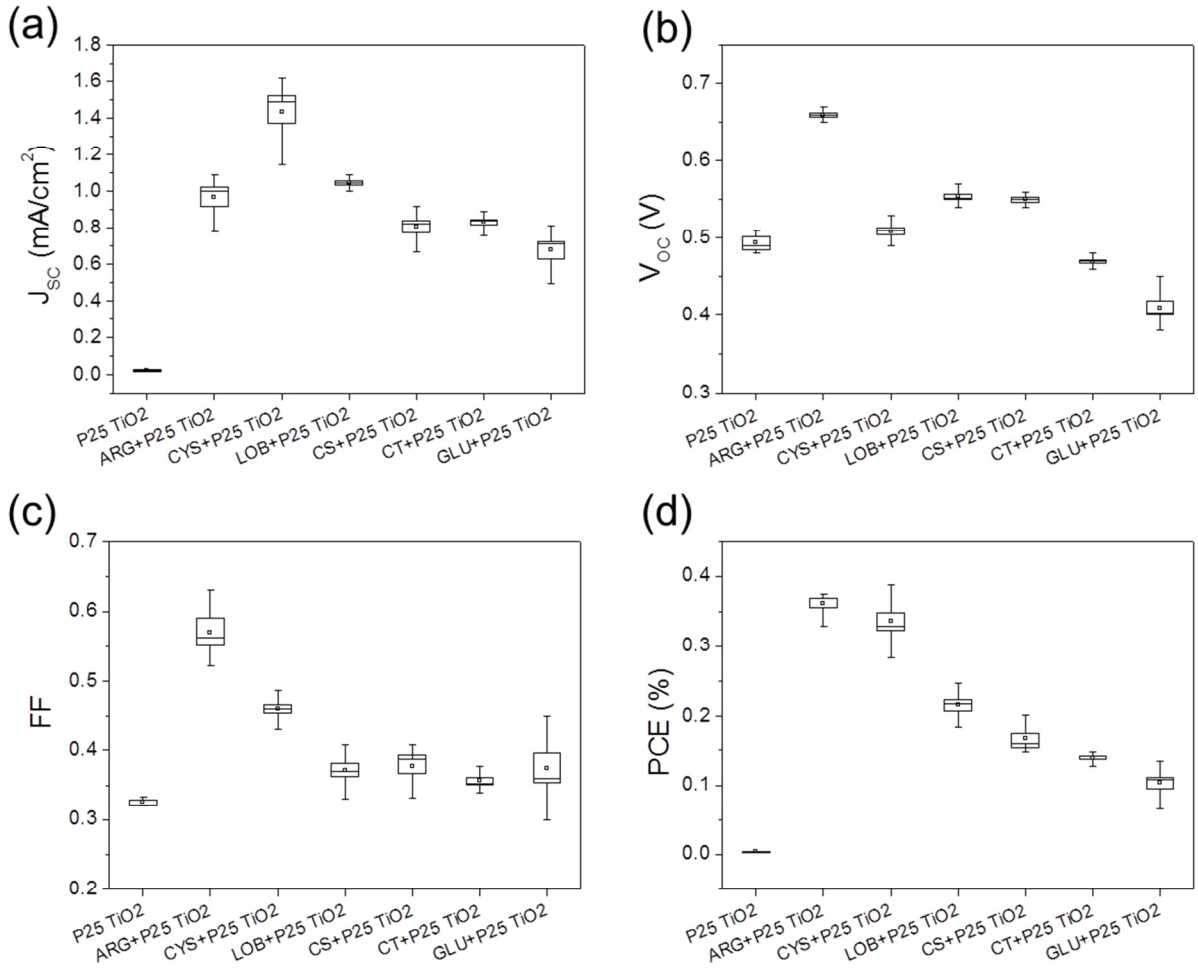

Figure 6 Box plots of key parameters for solar cells using carbon nanodots derived from L-arginine (ARG), L-cysteine (CYS), lobster shell (LOB), chitosan (CS), chitin (CT) and glucose (GLU): (a) short-circuit current density; (b) open-circuit voltage; (c) fill factor; (d) power conversion efficiency. Box represents standard error while whiskers represent max-min values.

The highest PCEs of the different CND-sensitised solar cells were produced by the amino-acid derived CNDs, with L-arginine giving (0.362 ± 0.007) % and L-cysteine (0.34 ± 0.01) %. These result from a combination of high J_{sc} values (up to (1.43 ± 0.06) mA/cm^2 for L-cysteine) with good V_{oc} and *FF* values. These can be partly attributed to the high R_{sh}, particularly for L-Arginine. The next best PCE value is produced by lobster-derived CNDs, with (0.216 ± 0.008) % as a result of high J_{sc} of (1.05 ± 0.01) mA/cm^2 and high V_{oc} coupled with R_s of only (0.48 ± 0.03) kΩ and moderate R_{sh} of (7.8 ± 0.2) kΩ. Finally, chitosan, chitin, and glucose CNDs give reducing PCEs in that order, as found in our previous study.[37] This correlates with increasing R_s and decreasing R_{sh}, the former potentially explaining the low J_{sc} for glucose.

In order to further investigate the origin of the variation in efficiency between CNDs derived from different precursors, the UV-Vis absorption of the CND-sensitised TiO_2 was measured, as shown in **Figure 7**. The sensitisation of the TiO_2 by the CNDs can be seen by the increase in light absorption across the 400-800 nm visible range, and particularly 400-600 nm. This correlates with light absorption from the visible absorption tail of the CNDs with onset ~700 nm, which can be seen more clearly in a close-up of the visible portion of their absorption (**Figure S7**). The strongest absorption of light is observed with D-glucose CNDs as sensitizers and the lowest light absorption is observed for chitin CNDs as sensitizers. This agrees with our previous findings[37] where we suggested that the high level of -OH and potentially carboxylic acid groups on glucose CNDs allows a high loading on the oxide surface, whereas the amide groups on chitin CNDs prevent good loading. However, lobster-derived CNDs, which were shown to also possess amide groups, show higher light absorption than chitin. This may suggest that the size of the CNDs may have an effect on loading: glucose and lobster produced the smallest CNDs (average 5.15 nm and 4.80 nm, respectively), therefore may diffuse within the pores of the TiO_2 more effectively than the larger CNDs, such as those derived from chitin (16.54 nm average diameter, see **SI, Table S1**). The complex interplay between CND size and functionalisation may therefore benefit from more in-depth investigation in future studies.

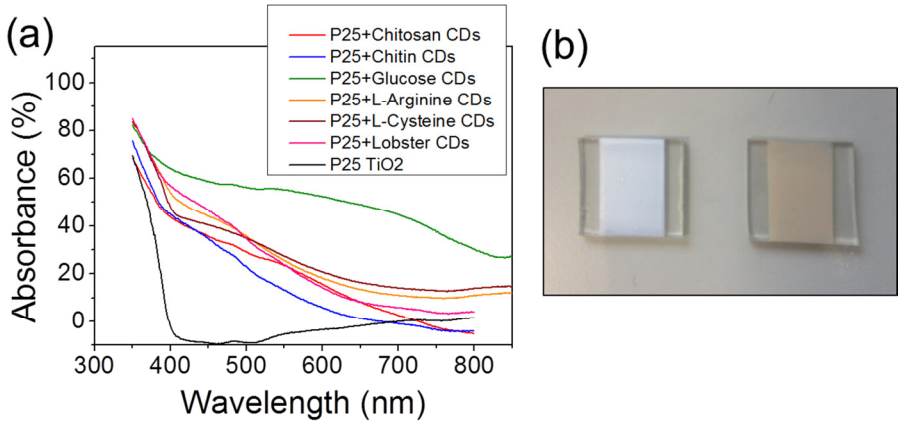

Figure 7 (a) Absorption spectra of TiO_2 (P25) sensitized with carbon nanodots. (b) Image of non-sensitized (left) and sensitized TiO_2 (P25) photoanode with carbon nanodots.

Looking at the data from **Figure 7** and **Table 1** we can see that there is low correlation between the light absorption of our CNDs as sensitizers and the solar cell performance parameters, particularly J_{sc}, which you would expect to correlate well with light absorption. For example, glucose CNDs have the highest light absorption, but the lowest J_{sc}, while the amino-acid-derived CNDs have the next highest light absorption and also among the highest J_{sc}. This suggests that the variation in performance of the solar cell devices is influenced by more than just the ability to harvest light as determined by CND loading and light absorption. Therefore the structural properties and nature of the sensitizers used, as determined by the functional groups present in the precursors, may also influence other factors, such as efficiency of charge collection due to differences in surface binding, charge transport and charge recombination (as supported by the large variation in internal resistance – **Table 1**).

We have therefore calculated the mean value of light harvesting efficiency (LHE) of solar cell devices (**Table 2**) in the range of 400-800 nm, from the absorption data given in **Figure 7,** allowing the average internal efficiency to also be calculated from the PCE (see Methods). These results demonstrate that the relatively high PCE of amino acid and lobster-derived CNDs results from a combination of high light harvesting with the highest internal efficiencies of all CNDs. Interestingly, although glucose CNDs as sensitizers show the highest LHE, their average internal efficiency is the lowest of all solar cell devices, leading to the lowest value of PCE of all solar cell devices. This is in agreement with a recent study that showed that increasing the visible absorption of CNDs in CNDSSCs did not increase the efficiency, since the states that produce the large visible tail (as seen in Figure 7 for glucose CNDs) result from trap states that do not contribute to the photocurrent[39]. Conversely, chitin CNDs have the lowest LHE, but show high average internal efficiency, leading to a moderate PCE. As would be expected, this indicates that a precursor which leads to CNDs with both good light harvesting properties and high internal efficiency in the solar cell (good charge transfer,

low internal and interfacial losses, *etc*.) will lead to the highest solar cell efficiencies. As discussed, within this sample set it seems that amino-acid derived CNDs have the best combination of these properties. The presence of thiol groups in the case of L-cysteine seems to have made little difference to the overall solar cell performance, although the V_{oc}-J_{sc} combination is slightly different to L-Arginine CNDs (**Figure 5** and **Figure 6**), possibly suggesting slightly different interactions within the solar cell. However, as discussed above, only a small proportion of thiol groups were retained in L-cysteine CNDs as indicated by the elemental analysis, therefore the functionality may be dominated by the amine groups. Thus, future investigation of other S-containing precursors may be necessary to identify whether it can affect performance. In addition, L-cysteine contains less amine groups than L-arginine, resulting in around half the N content in the final CNDs (**Table S5**). Therefore the difference in N content may also have influenced the performance. These results, however, do indicate that the functionality of amino acids is beneficial for CNDSSCs for at least two amino acids. Thus a more thorough screening of amino-acid-derived CNDs for this application in the future would help to elucidate the role of the different combinations of functionalities offered by this group of biologically-derived materials.

Table 2 Light harvesting efficiency (LHE), power conversion efficiency (PCE) and average internal efficiency of as-fabricated solar cells with commercial TiO_2 (P25).

Sample	**LHE (400-800 nm) [%]**	**Average internal efficiency [%]**	**PCE [%]**
Chitosan CNDs+P25	16.3	1.02 ± 0.05	0.167 ± 0.008
Chitin CNDs+P25	11.6	1.20 ± 0.02	0.139 ± 0.002
D-Glucose CNDs+P25	50.0	0.20 ± 0.02	0.103 ± 0.008
L-Arginine CNDs+P25	23.6	1.53 ± 0.03	0.362 ± 0.007
L-Cysteine CNDs+P25	24.5	1.39 ± 0.04	0.34 ± 0.01
Lobster CNDs+P25	20.8	1.04 ± 0.04	0.216 ± 0.008

Relating the functional groups present on the CND surface identified above with the differences in light harvesting and internal efficiency, a picture can be developed of how the CNDs interact with the TiO_2 surface, and how this affects the solar cell efficiency. UV-Vis absorption and LHE indicates that glucose CNDs adsorb most strongly to the TiO_2 surface. As discussed above and in our previous work,[37] the high concentration of alcohol and carboxylic acid functional groups on the surface of these

CNDs leads to strong bonding to the TiO_2 surface through bidentate-bridging and H-bonding, as is the case for common molecular dyes, such as N719.[45] However, as the proportion of these groups is so high, inter-molecular bonding is also promoted between the CNDs: glucose-derived CNDs were the only particles to show cluster formation in TEM analysis (Figure 1). They are therefore more likely to produce CND clusters on the TiO_2 surface. These clusters, combined with the possibility that the high visible absorption is associated with trap states[39] (as discussed above), would increase recombination in the glucose-derived CND devices as seen for dye clusters in DSSCs,[46] explaining the low internal efficiency despite high light absorption.

In the case of amino-acid-derived CNDs, these were shown to have a high proportion of amine groups present of the surface, which may lead to the high efficiency. However, chitosan CNDs also have amine groups present, and only demonstrate slightly higher efficiency than amide-containing chitin. This implies that it is the combination of carboxylic acid and amine functionalisation that is beneficial in the amino-acid-derived CNDs. Here, as discussed above, the carboxylic acid groups will aid anchoring and charge transfer to the TiO_2 surface, as used in traditional dye molecules such as N719.[45,47] This bonding is more efficient than that of amine groups, as shown in studies of dopamine bonding to the TiO_2 surface,[48] accounting for the higher LHE in amino-acid-derived CNDs compared to chitosan-derived CNDs. Then, compared to glucose-derived CNDs which contain C=O and –OH but no amines, the addition of amine groups appears to limit cluster formation, as no clusters were seen in TEM analysis of the amino-acid-derived CNDs. It is well-known that hydrogen bonding in amines is less efficient than for –OH containing molecules, which could account for the lower cluster formation where amine groups are present. In addition, the nitrogen functionalisation from amine groups may also alter the electronic states to reduce recombination in the CNDs, as many previous studies have shown that N-doping is beneficial for solar cell efficiency when using CNDs.[36,39,40] The precise role of nitrogen in increasing internal efficiency of such CNDs would thus be an excellent area for future study, for example by using spectroscopic techniques such as those used by Margraf *et al.* when studying their CNDSSCs.[39]

It is interesting to note that lobster CNDs demonstrate a similar internal efficiency to chitin and chitosan CNDs, but a LHE closer to the amino acids. Reviewing the XPS data for lobster CNDs, they contain a high level of C=O groups compared to other CNDs including chitin (**Figure 3** and **Figure S6**) combined with the expected amides, even though the purified lobster should largely similar to chitin, which does not contain C=O. They also have a much lower average diameter. This combination of small size and functionalisation more resembling the amino-acid-derived CNDs may increase the CND loading, leading to the higher LHE for these CNDs compared to those derived from pure chitin.

Thus, combining these findings, it is hypothesised that the most beneficial functional groups in a CND for optimum solar cell efficiency is a combination of carboxylic acid groups to encourage binding to the TiO_2 surface, coupled with groups which prevent cluster formation, such as amines or amides. Thus, in the set of precursor materials surveyed here, amino acids have the optimum combination of this functionalisation, which leads to the best combination of light harvesting and internal efficiency. It is further hypothesised that precursors which lead to functionalisation of CNDs with both carboxylic acids and amides, or other groups that prevent cluster formation, would display higher solar cell efficiency. Materials that contain this functionalisation would therefore be of interest for future studies into biomass-derived CNDs for this application.

However, in order to further increase efficiency, full understanding of the relationship between functional group, CND size, light absorption, surface adsorption and internal efficiency requires further study. With a wide range of potential structures and functionalisation, such further understanding could lead to specifically engineered carbon nanodots with LHE close to 100% in a given wavelength range (*e.g.* 400-900 nm), coupled with a high internal efficiency. Such developments should contribute to the development of carbon nanodot sensitized solar cell devices with efficiencies well above 1%.

Conclusions and Perspectives

We have used different biomass-derived precursors from the families of mono/polysaccharides (D-glucose, chitosan and chitin) and amino acids (L-arginine and L-cysteine) to prepare hydrothermally synthesized carbon nanodots as sensitizers for TiO_2 based solar cells. Also, for the first time in the literature, we have successfully used real food waste (lobster shells) to prepare carbon nanodots as sensitizers for TiO_2-based nanostructured solar cells. The as-synthesized carbon nanodots have been shown to contain different functional groups, which have origins in the starting precursors. These functional groups are responsible for the photoluminescence properties of carbon nanodots and the solar-cell performance appears to also be determined by structural/chemical properties of the as-synthesized carbon nanodots. While all types of carbon nanodots have successfully sensitized TiO_2 to visible light, the highest PCE of (0.362 ± 0.007) % was obtained by using L-arginine CNDs. Significantly, solar cells sensitised with CNDs produced from lobster shells gave an efficiency only slightly lower than this maximum value, of (0.216 ± 0.008) %.

This comparison of a variety of CNDs produced from a wide range of starting materials clearly demonstrates that the different combinations of functional groups present on the surface of carbon nanodots are a key factor for the performance of CND-sensitized TiO_2 solar cells. Both types of amino-acid-derived CNDs, which contain a high proportion of nitrogen in the form of amine groups combined with carboxylic acid groups, show the highest efficiencies. It is hypothesised that this leads

to the optimal combination of efficient binding to the TiO_2 surface via the carboxylic acid group leading to high light harvesting, with reduced cluster formation and internal recombination assisted by the nitrogen-containing amine group, increasing internal efficiency.

All these solar cell devices can be produced simply and cheaply by using solution methods. Furthermore, we have demonstrated that sensitizers produced from not only biomass, but specifically food waste could potentially be used in such nanostructured solar cells. However, their PCE needs further improvement to be a viable alternative to established and emerging solar cell devices. To achieve this, the light harvesting efficiency of carbon nanodots should be increased in the visible and NIR part of solar spectrum, while improving charge transfer processes and reducing recombination to increase the internal efficiency. This will require the investigation of a much wider range of possible biomass-derived precursors, including those with more diverse functionalities. This must be coupled with further developments in the understanding of the origins of the absorption and emission from these materials, obtained through fundamental studies, in order to identify possible routes to enhanced visible absorption. In addition, further optimisation of the solar cell structure, such as light-scattering layers and alternative electrolytes[38] and counter electrodes,[1] which were not used here, may also achieve higher efficiencies. With further understanding of the specific role of functional groups in the properties of carbon nanodots, as shown here to be of key importance, as well as other important factors such as anchoring on the TiO_2 surface, recombination processes, and the decoupling of effects related to functional groups, size, concentration etc., it should be possible to survey the huge range of potential biomass and waste-derived organic materials to identify those with the greatest potential to achieve the desired properties, and significantly increase device efficiency in the future.

Experimental methods

Chemicals

Chitin from shrimp shells (practical grade powder), chitosan (medium molecular weight), D-(+)-Glucose, L-Arginine (reagent grade), and L-Cysteine were all purchased from Sigma-Aldrich. Lobster was purchased from the food market in London, UK. Quinine sulphate was purchased from Acros Organics and H_2SO_4 was purchased from Sigma-Aldrich. Ethanol (ACS reagent, ≥99.8%) and acetone were both purchased from Sigma-Aldrich, and 2-Propanol from Fisher Chemical (assay ≥ 99.5%). Hydrochloric acid (assay 36.5-38%) was purchased from VWR Chemicals and sodium hydroxide (pellets, ≥98%) from Sigma-Aldrich. Titanium (IV) chloride (puriss, ≥99%) was purchased from Fluka Analytical, Pluronic-P123 (PEG-PPG-PEG) from Sigma-Aldrich and Acrodisc syringe filters from Pall Corporation. Titanium (IV) oxide (Aeroxide P25), ethyl cellulose (viscosity 10 cP and 46 cP), lauric acid and α–terpineol were all purchased from Sigma-Aldrich. All the chemicals were used without further purification.

Synthesis of Carbon Nanodots

Chitosan, chitin, D-(+)-Glucose, L-Arginine, L-Cysteine and purified lobster powder were all used as precursors for the hydrothermal synthesis of carbon nanodots. Briefly, 0.7 g of precursor was put in 20 mL of ethanol and placed in a stainless steel autoclave with Teflon inlet, which underwent hydrothermal treatment at 200 °C for 6 hours. After hydrothermal treatment the obtained liquid phase was centrifuged at 10,000 RPM for 15 min and then filtered through syringe filters (0.2 μm pore size) to obtain light yellow to dark brown solutions containing carbon nanodots. Purified lobster powder was obtained as follows. Lobster was purchased at the food market in London, UK. Then it was cooked, the meat was consumed and the shells were preserved. Shells were firstly soaked in NaOH (5 wt% compared to the mass of initial lobster shells) overnight at 70 °C, and then they were soaked in HCl solution (0.1 M) overnight at room temperature. As obtained purified lobster shells were stored in DI water in the fridge at 5 °C for the future use. Prior to their use in hydrothermal reaction, purified lobster shells were dried and milled into powder form. Purification procedure was done to remove soluble proteins and minerals from the lobster shells.

Fabrication of Carbon Nanodot Sensitized TiO_2 - based Nanostructured Solar Cells

2x2 cm glass substrates coated with fluorine doped tin oxide (FTO, Pilkington) were cleaned by sonicating them sequentially in acetone and 2-propanol for 15 min each. To form a TiO_2 compact layer on the FTO surface, the substrates were soaked in a mixture of 60 mL DI water and 0.22 mL of titanium (IV) chloride at 60 °C for 30 min. The substrates were then taken out and annealed on a hot plate at 450 °C for 30 min.

The TiO_2 paste was prepared as follows. 1g of titanium (IV) oxide (Aeroxide P25), 0.25g of ethyl cellulose (viscosity 10 cP), 0.25g of ethyl cellulose (viscosity 46 cP), 0.1g of lauric acid, 10 mL of ethanol and 3.33g of α-terpineol were all mixed together using pestle and mortar for 30 min until a thick white paste was obtained. The TiO_2 paste was doctor bladed on the $TiCl_4$-treated FTO-glass substrates and left at room temperature for 30 min, followed by annealing at 450 °C for 30 min. The TiO_2 layers were then treated with aqueous titanium (IV) chloride solution in the oven at 60 °C for 30 min, and re-annealed at 450 °C for 30 min. Sensitization of TiO_2 with carbon nanodots was achieved by putting glass substrates coated with TiO_2 into the CND solutions for 12 hours at 6 °C to allow the surface adsorption of the CNDs to saturate. [39]

Open-type cells were made by using Pt coated FTO glass substrate as a counter electrode, separated from the TiO_2 photoanode using a spacer, filled with I^-/I_3^- electrolyte solution (Iodolyte HI-30, Solaronix), and clamped shut.

Structural and Optical Characterisation

Transmission electron microscopy (TEM) was performed on JEOL JEM-2010 electron microscope operating at 200 kV. Carbon nanodots were dispersed in ethanol and one drop was applied onto the

copper grids coated with lacey carbon film (TAAB). Elemental analysis data were obtained by using Vario MICRO Cube elemental analyser system. Freeze dried carbon nanodots were obtained by using Scanvac Cool Safe 110-4 Pro freeze dryer operating at condenser temperature of -110 °C. Freeze dried carbon nanodots were used for the XPS, FTIR, Raman and XRD analysis. XPS measurements were performed on Specs spectrometer using Mg Kα (1253.6 eV) radiation from a double anode at 150 W. XPS binding energy values for carbon nanodots were charge-corrected placing the main C 1s peak at 285.5 eV. Fourier Transform Infrared Spectroscopy (FTIR) measurements were recorded by using Bruker Tensor 27 instrument equipped with diamond lens Attenuated Total Reflectance (ATR) module in the range from 4000 cm^{-1} to 400 cm^{-1}. Raman spectra were measured by using Renishaw 1000 microspectrometer with an excitation wavelength of 633 nm. X-ray diffraction (XRD) patterns were recorded using Panalytical Xpert Pro diffractometer equipped with Ni filtered Cu Kα radiation (λ_1=1.5406 Å and λ_2=1.5444 Å) collected in the 2θ range from 5° to 70°.

UV-Vis absorption spectra of carbon nanodot suspensions in ethanol (as used for solar cells) were recorded by using Perkin Elmer Lambda LS 35 UV-visible spectrometer. UV-Vis transmission and absorption spectra of TiO_2 sensitized with carbon nanodots were measured using a Perkin-Elmer Lambda 950 spectrometer fitted with an integrating sphere. The fluorescence spectra of carbon nanodot suspensions in ethanol were recorded using Perkin Elmer LS 55 fluorescence spectrometer. Slit width of 6 nm, both for excitation and emission spectra, was used when measuring fluorescence emission of aqueous solution of carbon nanodots. The excitation wavelength was increased from 200 nm to 480 nm in 20 nm increments and the corresponding fluorescence emission spectrum was recorded. Pure ethanol was used as a reference for all absorption, PL, and PLE measurements. Photoluminescence quantum yield (Φ) of carbon nanodots was determined by using quinine sulphate (QS) as a reference and following the procedure as described by Sahu *et al.*[49]

N_2 adsorption measurements of TiO_2 powder was performed at 77 K using Quantachrome Nova 4200e instrument. Prior to the measurements, the sample was degassed at 150 °C for 24 hours. Surface area was determined by applying the BET theory following the IUPAC procedure and the pore size distribution was obtained by fitting the isotherm to QSDFT adsorption kernel implemented in the NovaWin software provided by Quantachrome Instruments. High purity nitrogen gas was used for all the measurements.

Current-voltage Measurements of Solar Cell Devices

Current-voltage measurements of as produced TiO_2-based nanostructured solar cells sensitized with carbon nanodots were performed by using Keithley 2400 Source Meter SMU Instrument and 100 mW/cm^{-2} illumination (calibrated using a standard Si solar cell) using a Newport Oriel class ABB solar simulator with an AM 1.5 filter, all controlled by Labview software.

Average internal efficiency was estimated by dividing the power conversion efficiency (PCE) by the average light-harvesting efficiency (LHE). This estimation was used as the spectral external quantum efficiency (EQE, or incident photon-to-current efficiency, IPCE) could not be obtained due to low current output. The spectral EQE would therefore be an interesting addition to future studies of CNDSSCs if the current output can be increased, as it would indicate which wavelengths are contributing to the photocurrent.

Supporting Information is available, including: structural information of biomass precursors; full particle size data and additional TEM micrographs; additional XRD, Raman, FTIR and spectra with full breakdown and analysis of peaks; elemental analysis of as-produced CNDs; UV-Vis absorption data for CND solutions; full photoluminescence data for CND solutions; fluorescence quantum yields; fluorescence images of CND solutions; characterization of P25.

Acknowledgements

We would like to thank Dr Nadezda Tarakina assistance in obtaining TEM images, Dr Andrei Sapelkin and Nikolaos Papaioannou for the help with Raman measurements and Dr Rory Wilson for performing X-ray diffraction measurements.

References:

1. J. Briscoe and S. Dunn, *Advanced Materials*, 2016, **28**, 3802–3813.
2. W. Shockley and H. J. Queisser, *Journal of Applied Physics*, 1961, **32**, 510.
3. I. Hod and A. Zaban, *Langmuir*, 2014, **30**, 7264–7273.
4. M. Grätzel, *Journal of Photochemistry and Photobiology C: Photochemistry Reviews*, 2003, **4**, 145–153.
5. P. Peumans, A. Yakimov, and S. R. Forrest, *Journal of Applied Physics*, 2003, **93**, 3693.
6. S. Günes, H. Neugebauer, and N. S. Sariciftci, *Chemical Reviews*, 2007, **107**, 1324–1338.
7. N.-G. Park, *Materials Today*, 2015, **18**, 65–72.
8. R. Wang, Y. Shang, P. Kanjanaboos, W. Zhou, Z. Ning, and E. H. Sargent, *Energy Environ. Sci.*, 2016, **9**, 1130–1143.
9. A. Hagfeldt, G. Boschloo, L. Sun, L. Kloo, and H. Pettersson, *Chemical Reviews*, 2010, **110**,

6595–6663.

10. P. V. Kamat, *The Journal of Physical Chemistry Letters*, 2013, **4**, 908–918.

11. W. Li and X. Zhong, *The Journal of Physical Chemistry Letters*, 2015, **6**, 796–806.

12. Z. Pan, K. Zhao, J. Wang, H. Zhang, Y. Feng, and X. Zhong, *ACS Nano*, 2013, **7**, 5215–5222.

13. K. Zhao, Z. Pan, I. Mora-Seró, E. Cánovas, H. Wang, Y. Song, X. Gong, J. Wang, M. Bonn, J. Bisquert, and X. Zhong, *Journal of the American Chemical Society*, 2015, **137**, 5602–5609.

14. C.-H. M. Chuang, P. R. Brown, V. Bulović, and M. G. Bawendi, *Nature Materials*, 2014, **13**, 796–801.

15. S. Jiao, Q. Shen, I. Mora-Seró, J. Wang, Z. Pan, K. Zhao, Y. Kuga, X. Zhong, and J. Bisquert, *ACS Nano*, 2015, **9**, 908–915.

16. Y. C. Choi, D. U. Lee, J. H. Noh, E. K. Kim, and S. Il Seok, *Advanced Functional Materials*, 2014, **24**, 3587–3592.

17. Z. Ren, J. Wang, Z. Pan, K. Zhao, H. Zhang, Y. Li, Y. Zhao, I. Mora-Sero, J. Bisquert, and X. Zhong, *Chemistry of Materials*, 2015, **27**, 8398–8405.

18. Z. Ren, Z. Wang, R. Wang, Z. Pan, X. Gong, and X. Zhong, *Chemistry of Materials*, 2016, **28**, 2323–2330.

19. J. Wang, Y. Li, Q. Shen, T. Izuishi, Z. Pan, K. Zhao, and X. Zhong, *J. Mater. Chem. A*, 2016, **4**, 877–886.

20. Z. Du, Z. Pan, F. Fabregat-Santiago, K. Zhao, D. Long, H. Zhang, Y. Zhao, X. Zhong, J.-S. Yu, and J. Bisquert, *The Journal of Physical Chemistry Letters*, 2016, **7**, 3103–3111.

21. I. Robel, V. Subramanian, M. Kuno, and P. V. Kamat, *Journal of the American Chemical Society*, 2006, **128**, 2385–2393.

22. I. J. Kramer and E. H. Sargent, *Chemical Reviews*, 2014, **114**, 863–882.

23. J. Du, Z. Du, J.-S. Hu, Z. Pan, Q. Shen, J. Sun, D. Long, H. Dong, L. Sun, X. Zhong, and L.-J. Wan, *Journal of the American Chemical Society*, 2016, **138**, 4201–4209.

24. S. Y. Lim, W. Shen, and Z. Gao, *Chem. Soc. Rev.*, 2015, **44**, 362–381.

25. H. Li, Z. Kang, Y. Liu, and S.-T. Lee, *Journal of Materials Chemistry*, 2012, **22**, 24230.

26. X. Li, M. Rui, J. Song, Z. Shen, and H. Zeng, *Advanced Functional Materials*, 2015, **25**,

4929–4947.

27. Y. Wang and A. Hu, *Journal of Materials Chemistry C*, 2014, **2**, 6921.

28. R. J. White, N. Yoshizawa, M. Antonietti, and M.-M. Titirici, *Green Chemistry*, 2011, **13**, 2428.

29. R. J. White, M. Antonietti, and M.-M. Titirici, *Journal of Materials Chemistry*, 2009, **19**, 8645.

30. S. Liu, J. Q. Tian, L. Wang, Y. W. Zhang, X. Y. Qin, Y. L. Luo, A. M. Asiri, A. O. Al-Youbi, and X. P. Sun, *Advanced Materials*, 2012, **24**, 2037–2041.

31. N. Dhenadhayalan, K.-C. Lin, R. Suresh, and P. Ramamurthy, *The Journal of Physical Chemistry C*, 2016, **120**, 1252–1261.

32. H. Ding, S.-B. Yu, J.-S. Wei, and H.-M. Xiong, *ACS Nano*, 2016, **10**, 484–491.

33. L. Wang, S.-J. Zhu, H.-Y. Wang, S.-N. Qu, Y.-L. Zhang, J.-H. Zhang, Q.-D. Chen, H.-L. Xu, W. Han, B. Yang, and H.-B. Sun, *ACS Nano*, 2014, **8**, 2541–2547.

34. X. Yan, X. Cui, B. Li, and L. Li, *Nano Letters*, 2010, **10**, 1869–1873.

35. P. Mirtchev, E. J. Henderson, N. Soheilnia, C. M. Yip, and G. a. Ozin, *Journal of Materials Chemistry*, 2012, **22**, 1265.

36. Y.-Q. Zhang, D.-K. Ma, Y.-G. Zhang, W. Chen, and S.-M. Huang, *Nano Energy*, 2013, **2**, 545–552.

37. J. Briscoe, A. Marinovic, M. Sevilla, S. Dunn, and M. Titirici, *Angewandte Chemie International Edition*, 2015, **54**, 4463–4468.

38. H. Zhang, Y. Wang, P. Liu, Y. Li, H. G. Yang, T. An, P. Wong, D. Wang, Z. Tang, and H. Zhao, *Nano Energy*, 2015, **13**, 124–130.

39. J. T. Margraf, F. Lodermeyer, V. Strauss, P. Haines, J. Walter, W. Peukert, R. D. Costa, T. Clark, and D. M. Guldi, *Nanoscale Horiz.*, 2016.

40. H. Wang, P. Sun, S. Cong, J. Wu, L. Gao, Y. Wang, X. Dai, Q. Yi, and G. Zou, *Nanoscale Research Letters*, 2016, **11**, 27.

41. F. Tuinstra and J. L. Koenig, *The Journal of Chemical Physics*, 1970, **53**.

42. R. P. Vidano, D. B. Fischbach, L. J. Willis, and T. M. Loehr, *Solid State Communications*,

1981, **39**, 341–344.

43. S. Zhu, Q. Meng, L. Wang, J. Zhang, Y. Song, H. Jin, K. Zhang, H. Sun, H. Wang, and B. Yang, *Angew Chem Int Ed Engl*, 2013, **52**, 3953–3957.

44. D. Qu, M. Zheng, L. Zhang, H. Zhao, Z. Xie, X. Jing, R. E. Haddad, H. Fan, and Z. Sun, *Scientific Reports*, 2014, **4**, 5294.

45. K. E. Lee, M. A. Gomez, S. Elouatik, and G. P. Demopoulos, *Langmuir*, 2010, **26**, 9575–9583.

46. H. J. Snaith and L. Schmidt-Mende, *Advanced Materials*, 2007, **19**, 3187–3200.

47. H. Wang, D.-W. Zhang, and Z.-T. Li, in *Hydrogen Bonded Supramolecular Materials*, eds. Z.-T. Li and L.-Z. Wu, Springer, 2015, pp. 185–231.

48. M. J. Jackman, K. L. Syres, D. J. H. Cant, S. J. O. Hardman, and A. G. Thomas, *Langmuir*, 2014, **30**, 8761–8769.

49. S. Sahu, B. Behera, T. K. Maiti, and S. Mohapatra, *Chemical Communications*, 2012, **48**, 8835–8837.